ChemComm

Accepted Manuscript

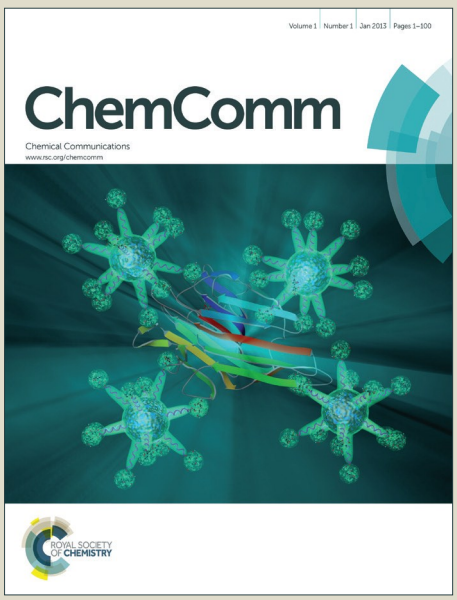

ROYAL SOCIETY OF CHEMISTRY

www.rsc.org/chemcomm

Journal Name

COMMUNICATION

A "Uniform" Heterogeneous Photocatalyst: Integrated P-N Type $CuInS_2/NaInS_2$ Nanosheets by Partial Ion Exchange Reaction for Efficient H_2 Evolution

Received 00th January 20xx,
Accepted 00th January 20xx

DOI: 10.1039/x0xx00000x

www.rsc.org/

Peng Hu,[a,e] Chee Keong Ngaw,[a,b] Yee Yan Tay,[a,c] Shaowen Cao,[a] James Barber,[a,d] Timothy Thatt Yang Tan*[b] Say Chye Joachim Loo*[a]

Single-crystalline-like P-N type $CuInS_2/NaInS_2$ heterogeneous nanosheets were synthesized by partial cation exchange reaction and show highly improved photocatalytic H_2 evolution activity attributed to the increased efficiency of interfacial charge transfer.

Nanocomposites with integrated functional components can be endowed with superior properties beyond that of their parent materials, thus enhancing their performances for different applications.[1] A typical example is heterogeneous p-n type photocatalysts, in which the integrated semiconductor pair forms a stepwise bandgap alignment. Such heterostructures favour carrier separation and transport to different counterparts, inhibiting electron-hole recombination, thus improving their photoelectric properties.[2] Generally, heterostructured photocatalysts are constructed by sequential growth of secondary nanoparticles on the surface of the parent semiconductor. This construction strategy focuses on suppressing homogeneous nucleation of secondary materials that will compete with the desired heterogeneous nucleation on the existing nanocrystal surface. However, integrating highly disparate materials together at the nanoscale level is not trivial, yet achieving well-defined size, morphology and interface, which are critical for efficient charge cascading process in photocatalytic reactions. Achieving this would realize efficient carrier transportation that improves photocatalytic performance.[3]

In binary ionic metal chalcogenides, cation exchange reactions have been demonstrated to be a simple and efficient method to precisely modify the composition and properties of nanocrystals, while providing controlled morphology.[4] We have demonstrated a cation-exchange strategy to synthesize ternary sulphide nanorings with a significantly enhanced visible-light-driven photocatalytic activity for H_2 evolution.[5] In isovalent metal chalcogenides, solid solution nanostructures are mostly obtained by partial cation exchange reactions.[6] Nonetheless, recent work also showed that secondary heterostructures can be created from CdS nanocrystals with aliovalent metal cations. For example, CdS/Ag_2S, CdS/Cu_2S, CdS/PbS heterostructures can be obtained by partial cation exchange reaction between CdS with the corresponding ions (note that CdS/PbS heterostructures are formed by partial exchange of aliovalent Cu^+ then Pb^{2+}).[7] The atom-level interface makes it possible to efficiently tune the carrier distribution in individual components, thus rendering new electrical properties.[8] This strategy is a promising approach in designing novel heterogeneous photocatalysts with improved performances. However, there is a dearth of reports on such a strategy, for fabrication of metal chalcogenides heterostructures with suitable band offset.

Here, the formation of atomic-level integrated heterostructures composed of ternary sulphides by adopting the partial cation exchange reaction is reported for the first time. N-type $NaInS_2$ and P-type $CuInS_2$ were selected to illustrate a fully integrated heterostructure within a single nanosheet. The morphological evolution from aggregated nanosheets to two-dimensional monodisperse nanosheets was observed during cation exchange reactions. Synthesized *in situ* heterogeneous photocatalyst with low crystal defect was found to inhibit interfacial charge recombination, subsequently resulting in high photocatalytic H_2 evolution rates.

$NaInS_2$ nanocrystals were synthesized by a solvothermal reaction between $InCl_3$ and $Na_2S{\cdot}2H_2O$ in a mixed solution of ethanol and methanol. The as-synthesized products were first analyzed by a field-emission scanning electron microscopy (FESEM) and transmission electron microscopy (TEM), as shown in Figures 1a and 1b. It was observed that the products were round-shaped nanosheets of diameter ~1 μm. A second-order growth on the centre surface of the primary nanosheets also occurred in some nanocrystals. Typical morphological evolution of $NaInS_2$ nanoparticles with different reaction times was also investigated as shown in Figure S1. When Cu^+

[a] Solar Fuels Lab, School of Materials Science and Engineering, Nanyang technological University, 50 Nanyang Avenue, 639798 Singapore, E-mail: joachimloo@ntu.edu.sg.
[b] Solar Fuels Lab, School of Chemical and Biomedical Engineering, Nanyang technological University, 62 Nanyang Drive, 637459 Singapore, E-mail: tytan@ntu.edu.sg.
[c] Facility for Analysis, Characterization, Testing and Simulation, Nanyang technological University, 50 Nanyang Avenue, 639798, Singapore
[d] Division of Molecular Bioscience, Department of Life Science, Imperial College London, SW7 2AZ, UK
[e] State Key Laboratory of Multiphase Complex Systems, Institute of Processing Engineering, Chinese Academy of Sciences, Beijing, 100190, China.
Electronic Supplementary Information (ESI) available: [details of any supplementary information available should be included here]. See DOI: 10.1039/x0xx00000x

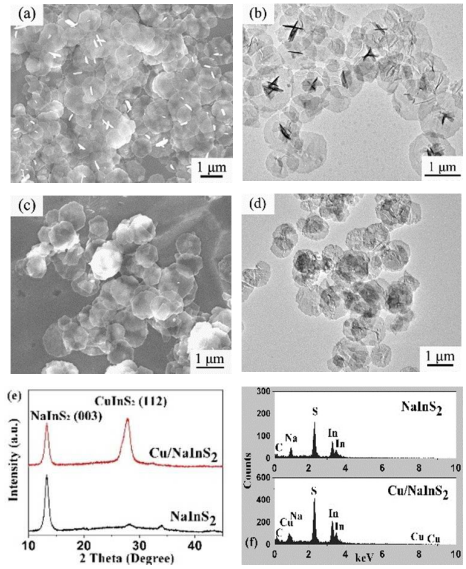

Fig. 1 (a) SEM and (b) TEM images of pure $NaInS_2$ nanosheets. (c) SEM and (d) TEM images of $CuInS_2/NaInS_2$ nanosheets obtained after Cu^+ ions exchange. (e) XRD patterns of $NaInS_2$and $CuInS_2/NaInS_2$ nanosheets. (f) EDS spectra for the synthesized $NaInS_2$and $CuInS_2/NaInS_2$ nanosheets.

ions were introduced to $NaInS_2$ precursor at room temperature, a colour change from yellow to brown was immediately observed (≤1s), and a morphological evolution from aggregated nanosheets to monodisperse two-dimensional nanostructure was also observed (Figure S2a, b). X-ray diffraction (XRD), UV-vis absorption spectra and energy-dispersive X-ray spectroscopy (EDS) analyses confirmed that non-crystalline $CuInS_2$ had been formed in the $NaInS_2$ nanosheets (Figure S2 c-e).

After hydrothermal treatment, no obvious shape change was observed from both SEM and TEM images (Figures 1c and d), but structural analysis revealed the emergence of a new peak located at 27.9° in the XRD pattern of $Cu/NaInS_2$ compared to pure $NaInS_2$ (Figure 1e). Pure $NaInS_2$ can be indexed to rhombohedral $NaInS_2$ phase (JPDS No.74-0135) with a strong diffraction peak of (003), while pure tetragonal $CuInS_2$ can be indexed to (112) peak located at 27.9° (JPDS No.82-1702). The emergence of a new $CuInS_2$ (112) peak after the reaction, with the preservation of the $NaInS_2$ (003) peak, strongly suggest a structural change from a pure $NaInS_2$ phase to a mixture of rhombohedral $NaInS_2$ and tetragonal $CuInS_2$ phases. This confirms the formation of integrated $NaInS_2/CuInS_2$ heterogeneous nanosheets. Structural evolution of this integration was verified by XRD with different amounts of Cu^+ ions (Figure S3). The intensity ratio of the (112) to (003) peaks increased with increasing Cu^+ content, until pure $CuInS_2$ nanosheets were obtained. EDS (Figure1f) and inductively coupled plasma atomic emission spectrometer analyses (ICP-AES, Table S1) of the products were consistent with full elemental composition after Cu^+ exchange.

The detailed structure of the synthesized $NaInS_2/CuInS_2$ heterogeneous nanosheets was further investigated by TEM, high-resolution TEM (HRTEM) and EDS elemental mapping. A rough surface could be observed from TEM (Figure 2a), caused by the removal of NaCl formed during the synthesis of $NaInS_2$. Elemental mapping (Figure 2b) revealed the composition and elemental distribution of the nanosheets. The nanosheets were mainly composed of uniformly distributed S, In, Na and Cu. Different areas on the nanosheets were further investigated by HRTEM for detailed structural information. Figure 2c shows the typical TEM image of the heterosheets, and the striped pattern observed was from Cu^+ exchange.[9] HRTEM imaging showed a single-crystalline structure. The measured lattice spacing of the adjacent planes was 0.38 nm, corresponding to the (220) plane distance of $NaInS_2$ crystal (Figure S4), which is also in accordance with the selected area electron diffraction (SAED) (inset in Figure 2c). These results revealed that no obvious lattice mismatch existed between the two different compounds in these nanosheets.

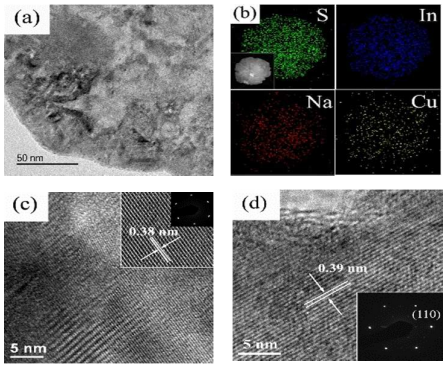

Fig.2 (a) TEM image and (b) EDS elemental maps of the heterogeneous nanosheet, (c) HRTEM image of $NaInS_2/CuInS_2$ heterogeneous nanosheet and (d) HRTEM image of $CuInS_2$ nanosheet after complete cation exchange.

To further understand the structure of the heterogeneous constructs, $CuInS_2$ nanosheets obtained by complete cation exchange reaction were observed under HRTEM (Figure 2d). A single crystal structure with exposed lattice space of 0.39 nm was observed, which is similar to the lattice space of $NaInS_2$ (220) plane (0.38 nm). As a result, no obvious lattice mismatch was observed in heterogeneous nanosheets. During the cation exchange reaction, dissolution and re-association reactions occurred simultaneously over a small length scale of reaction zone,[10] allowing structural transformation from the parent to the resulting crystals, thereby preserving the original crystallographic information.[11]

In a cation exchange reaction, the formation of a solid solution *versus* a two-component heterostructure was distinguished by the mutual solubility limits of both phases, as well as their interfacial energies.[8] In this case, the much higher solubility of Na^+ compared to that of Cu^+ ion favours heterostructured formation, which is also the thermodynamic driving force for the exchange reaction. The interfacial energy is mainly determined by the elastic strain and the chemical formation energy of different crystalline facets exposed at the surface of the crystals. Both contributions have been applied to explain the superlattice pattern of Ag_2S and end-attachment of Cu_2S in CdS nanorods.[7c, 9a] Due to minimal mismatch of the lattice space between (220) plane of $NaInS_2$ (0.38 nm) and (110) plane of $CuInS_2$

(0.39 nm), the elastic contributions are small for the interfacial energy, which is mainly determined by the chemical formation energies of the $CuInS_2$ crystalline facet. Schematic illustration of the atom arrangement analysis shows that the formed $CuInS_2$ nanocrystals revealed similar layer structure with $NaInS_2$ (Figure S5), which is a close-packed arrangement with minimum surface energy difference. Thus, the formation energy of these crystal facet gives a preference for interfacial nucleation and growth of a stable secondary $CuInS_2$ phase within the $NaInS_2$ nanocrystal, rather than the formation of a solid solution ($Cu_xNa_{1-x}InS_2$), which would otherwise change the crystal lattice and increase surface energy of the products due to difference in the ion sizes.[5]

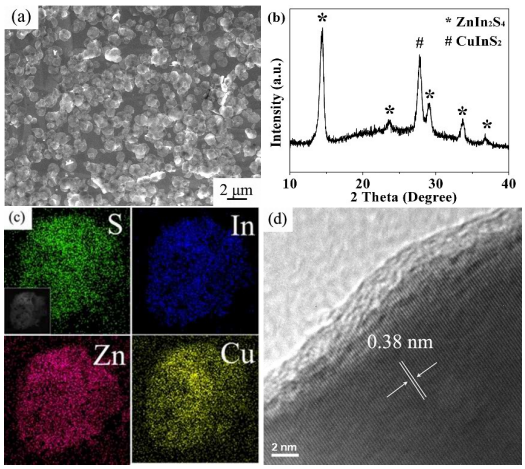

Fig.3 (a) SEM image, (b) XRD pattern, (c) EDS elemental maps and (d) HRTEM image of obtained $ZnIn_2S_4/CuInS_2$ nanosheets.

The components of the heterogeneous nanosheets could be further adjusted by multi-cation exchange. Figure 3 shows the morphology and structure analysis of $ZnIn_2S_4/CuInS_2$ heterogeneous nanosheets synthesized by a multi-cation exchange of Zn^{2+} and Cu^{+}. Two-dimensional monodisperse nanosheets still dominated as shown in Figure 3a. XRD pattern in Figure 3b confirmed the formation of $ZnIn_2S_4/CuInS_2$heterogeneous structure, and the S, In, Zn and Cu were uniformly distributed in the nanosheets (Figure 3c). The HRTEM image in Figure 3d illustrates the single-crystalline structure of the products, and the measured fringe spacing is 0.38 nm, corresponding to the (220) interplanar distance of the $ZnIn_2S_4$. The feasibility of the current synthetic strategy to prepare other integrated heterostructures is further demonstrated by fabricating $CuInS_2/MgIn_2S_4$, $ZnIn_2S_4/MgIn_2S_4$ and $NaInS_2/MgIn_2S_4$ (Figure S6).

Controlling the volume fraction of two crystals in the nanosheets made it possible to adjust the optical and electrical properties of synthesized heterostructures. The UV-vis absorption spectra of heterogeneous $CuInS_2/NaInS_2$ nanosheets were investigated, and enhanced visible light absorption was observed for these heterogeneous nanosheets with increasing amount of $CuInS_2$ nanocrystals (Figure S7). Figure 4a shows the visible-light-driven photocatalytic H_2 evolution activities of the $CuInS_2/NaInS_2$ nanosheets with different molar ratio of Cu/Na (in the absence of co- catalyst). It was observed that the heterogeneous nanosheets with low Cu^{+} ions showed remarkable photocatalytic activities than that

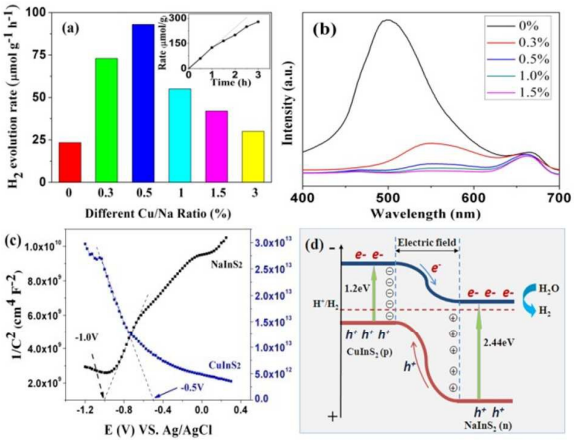

Fig.4 (a) Specific photocatalytic H_2 evolution rates and of as-synthesized heterostructures under visible-light (λ > 420 nm), inset shows the time-dependent photocatalytic H_2 evolution rate of the 0.5% Cu exchange $NaInS_2$ nanosheets, (b) PL spectra of heterostructured nanosheets with different molar ratio of Cu/Na, (c) flatband potentials of pure $NaInS_2$ and $CuInS_2$, (d) bandgap structure of integrated heterogeneous $NaInS_2/CuInS_2$ nanosheets.

of pure $NaInS_2$. The highest photocatalytic H_2 evolution rate of ~93μmol·g^{-1}·h^{-1} could be obtained from the sample with 0.5 % Cu^{+} ions, which is about 4.2 times higher than pure $NaInS_2$ nanosheets. Further increasing the extent of ion exchange led to a reduction of the photocatalytic H_2 production rate. Inset of Figure 4a shows the time-dependent photocatalytic H_2 evolution rate of the 0.5% Cu exchange $NaInS_2$ nanosheets. A decrease in production rate can be observed after 3 h. Although the oxidization process could be considerably suppressed in the presence of sacrificial reagents, photocorrosion will still occur, and efficiency will decrease with time, especially for sulfide nanomaterials without sulfide sacrificial reagents such as Na_2SO_3.

Photoluminescence (PL) spectra of the products were shown in Figure 4b. The peak intensity of nanosheets decreased sharply when Cu^{+} was first introduced, and gradually decreased when Cu^{+} was higher than 0.5%. The band gap of $NaInS_2$ is about 2.3–3.4 eV, and thus the peak nears 500 nm can be attributed to the near-band-edge emission. The PL peak of $NaInS_2/CuInS_2$ heterostructures exhibited a red-shift and broadened with increasing $CuInS_2$. These could be attributed to the formation of the $NaInS_2/CuInS_2$ interface, which could result in band bending due to the formation of interface states of the excitons. Along with extrinsic self-trapping of excitons with lattice distortion, a red-shift and broadening of the $CuInS_2$ PL peak would be observed.[12] The low PL intensity could be attributed to a reduction in the rate of carrier recombination,[13], suggesting a higher efficiency of carrier separation for these heterogeneous nanosheets.

To further understand the role of $NaInS_2/CuInS_2$ heterostructures in promoting photocatalytic reaction, bandgap structures of $NaInS_2$ and fully ion-exchanged $CuInS_2$ were investigated. First, the bandgap energy of pure $NaInS_2$ and $CuInS_2$ were calculated based on the UV-vis diffuse reflectance spectra, and determined to be 2.44 eV and 1.20 eV, respectively (Figure S8a and b). The semiconducting type and flatband potentials of individual materials

were obtained from Mott-Schottky measurement as shown in Figure 4c. From the curves, $NaInS_2$ and $CuInS_2$ were determined to be n-type and p-type semiconductors, and their flatband potentials were -1.0 and –0.5 V vs Ag/AgCl at pH=12, or -0.151 V and 0.439 V vs NHE at pH=0, respectively. Bandgap structure of the heterogeneous $NaInS_2/CuInS_2$ nanosheets could be obtained, as shown in Figure 4d. From the images, the cascading bandgap alignment was formed between the two nanocrystals. During photocatalytic process, the photo reduction reaction that occurred on the surface of $NaInS_2$ was remarkably enhanced, due to enhanced charge separation and low charge recombination from the build-in electric field at the p-n junction.[14] When $CuInS_2$ was further increased, active sites on the surface of $NaInS_2$ would be covered by $CuInS_2$ nanocrystals, preventing the generation of photoexcited electrons. This led to a reduction of H_2 evolution rates for Cu^+ higher than 0.5%.

In heterostructured photocatalysts, an efficient interfacial area is critical for photogenerated carrier transfer. It has been shown that co-catalysts formed in atomic clusters are more efficient than nanoparticle size-range in promoting photocatalytic properties.[15] Here, $CuInS_2$ is fully integrated into the nanocrystals, which functioned as cluster-like co-catalyst, thus providing efficient atomic-level interfacial contact and carrier transfer between the nanoscale phases. This leads to superior properties compared to that of hetereostructures formed from sequentially-grown nanoparticles-based composites (control with 0.5 % $CuInS_2$ nanoparticles decorated on $NaInS_2$ nanosheets were performed, Figure S9). Nanoparticles-sensitized heterocatalysts displayed a photocatalytic H_2 evolution rate of about 26 $\mu mol \cdot g^{-1} \cdot h^{-1}$, which is significantly lower than that of integrated heterostructured photocatalysts.

Time-dependent photocurrents were further analysed for pure $NaInS_2$, 0.5% $CuInS_2$ nanoparticles decorated $NaInS_2$ nanosheets and 0.5% $CuInS_2$ integrated $NaInS_2$ heterostructures (Figure S10), and the latter exhibited the highest current response. Photocurrent results were consistent with the photocatalytic H_2 evolution rate, and their transient time constants were calculated as 2.15s, 2.40s and 6.55s respectively. These results confirmed the efficient carrier transportation of the synthesized $CuInS_2/NaInS_2$ heterostructures.

Conclusions

This work reports on a facile strategy to fabricate integrated heterogeneous photocatalysts in ternary sulfides by an *in situ* partial ion-exchange reaction. The volume fraction of two crystals within the heterostructured nanosheets could be tuned by controlling the extent of the cation exchange reactions. The resulting heterogeneous nanosheets demonstrated high visible-light-driven photocatalytic activity with efficient H_2 evolution in water splitting, attributed to an efficient carrier separation from the built-in electric field between the p-n interfaces. The current synthesis strategy opens a promising approach to design and fabricate novel heterogeneous photocatalysts with precisely tunable structures and properties for enhanced performance in photoelectric applications.

Notes and references

‡ The authors would like to acknowledge the financial support from the NTU Solar Fuels Laboratory.

1 (a) F. Guo, B. Yang, Y. Yuan, Z. Xiao, Q. Dong, Y. Bi, J. Huang, *Nat. Nano.,* 2012, **7**, 798-802; (b) R. Mezzenga, J. Ruokolainen, *Nat. Mater.,* 2009, **8**, 926-928; (c) B. Poudel, Q. Hao, Y. Ma, Y. Lan, A. Minnich, B. Yu, X. Yan, D. Wang, A. Muto, D. Vashaee, X. Chen, J. Liu, M. S. Dresselhaus, G. Chen, Z. Ren, *Science,* 2008, **320**, 634-638; (d) L. Yang, S. Cheng, Y. Ding, X. Zhu, Z. L. Wang, M. Liu, *Nano Lett.,* 2011, **12**, 321-325; (e) M.Q. Yang, N. Zhang, M. Pagliaro, Y.J. Xu, *Chem. Soc. Rev.,* 2014, **43**, 8240-8254.

2 (a) M.R. Gao, Y.F. Xu, J. Jiang, Y.R. Zheng, S.H. Yu, *J. Am. Chem. Soc.,* 2012, **134**, 2930-2933; (b) A. Kudo, Y. Miseki, *Chem. Soc. Rev.,* 2009, **38**, 253-278; (c) J. Xu, C.Y. Luan, Y.B. Tang, X. Chen, J. A. Zapien, W.J. Zhang, H.L. Kwong, X.M. Meng, S.T. Lee, C.S. Lee, *ACS Nano,* 2010, **4**, 6064-6070; (d) Z. Yin, Z. Wang, Y. Du, X. Qi, Y. Huang, C. Xue, H. Zhang, *Adv. Mater.,* 2012, **24**, 5374-5378; (e) C. Liu, J. Tang, H. M. Chen, B. Liu, P. Yang, *Nano Lett.,* 2013, **13**, 2989-2992; (f) S. C. Roy, O. K. Varghese, M. Paulose, C. A. Grimes, *ACS Nano,* 2010, **4**, 1259-1278; (g) H. Tada, T. Mitsui, T. Kiyonaga, T. Akita, K. Tanaka, *Nat. Mater.,* 2006, **5**, 782-786; (h) S. I. In, D. D. Vaughn, R. E. Schaak, *Angew. Chem. Int. Ed.,* 2012, **51**, 3915-3918.

3 (a) Q. Xiang, J. Yu, M. Jaroniec, *J. Am. Chem. Soc.,* 2012, **134**, 6575-6578; (b) N. Zhang, Y. Zhang, Y.J. Xu, *Nanoscale,* 2012, **4**, 5792-5813.

4 (a) B. Zhang, Y. Jung, H.S. Chung, L. V. Vugt, R. Agarwal, *Nano Lett.,* 2009, **10**, 149-155; (b) P. K. Jain, L. Amirav, S. Aloni, A. P. Alivisatos, *J. Am. Chem. Soc.,* 2010, **132**, 9997-9999; (c) Q. Yao, I. U. Arachchige, S. L. Brock, *J. Am. Chem. Soc.,* 2009, **131**, 2800-2801.

5 P. Hu, S. S. Pramana, S. Cao, C. K. Ngaw, J. Lin, S. C. J. Loo, T. T. Y. Tan, *Adv. Mater.,* 2013, **25**, 2567-2572.

6 (a) Y. Yu, J. Zhang, X. Wu, W. Zhao, B. Zhang, *Angew. Chem. Int. Ed.,*2012, **51**, 897-900; (b) X. Wu, Y. Yu, Y. Liu, Y. Xu, C. Liu, B. Zhang, *Angew. Chem. Int. Ed.,* 2012, 51, 3211-3215.

7 (a) J. M. Luther, H. Zheng, B. Sadtler, A. P. Alivisatos, *J. Am. Chem. Soc.,* 2009, **131**, 16851-16857; (b) D. O. Demchenko, R. D. Robinson, B. Sadtler, C. K. Erdonmez, A. P. Alivisatos, L.W. Wang, *ACS Nano,* 2008, **2**, 627-636; (c) B. Sadtler, D. O. Demchenko, H. Zheng, S. M. Hughes, M. G. Merkle, U. Dahmen, L. W. Wang, A. P. Alivisatos, *J. Am. Chem. Soc.,* 2009, **131**, 5285-5293.

8 J. B. Rivest, P. K. Jain, *Chem. Soc. Rev.,* 2013, **42**, 89-96.

9 (a) R. D. Robinson, B. Sadtler, D. O. Demchenko, C. K. Erdonmez, L.W. Wang, A. P. Alivisatos, *Science,* 2007, **317**, 355-358; (b) S. Kudera, L. Carbone, M. F. Casula, R. Cingolani, A. Falqui, E. Snoeck, W. J. Parak, L. Manna, *Nano Lett.,* 2005, **5**, 445-449.

10 D. H. Son, S. M. Hughes, Y. Yin, A. Paul Alivisatos, *Science,* 2004, **306**, 1009-1012.

11 A. Putnis, *Miner. Mag.,* 2002, **66**, 689-708.

12 (a) L. H. Lin, X. Z. Sun, R. Tao, Z. C. Li, J. Y. Feng, Z. J. Zhang, *J. Appl. Phys.,* 2011, **110**, 073109; (b) Z. Xiong, M. Zheng, H. Li, L. Ma, W. Shen, *Mater. Lett.,* 2013, **112**, 211-214.

13 S. Shen, L. Zhao, Z. Zhou, L. Guo, *J. Phys. Chem. C,* 2008, **112**, 16148-16155.

14 (a) J. Zhang, J. Yu, Y. Zhang, Q. Li, J. R. Gong, *Nano Lett.,* 2011, **11**, 4774-4779; (b) X. Wang, Q. Xu, M. Li, S. Shen, X. Wang, Y. Wang, Z. Feng, J. Shi, H. Han, C. Li, *Angew. Chem. Int. Ed.,* 2012, **51**, 13180-13180.

15 (a) F. F. Schweinberger, M. J. Berr, M. Döblinger, C. Wolff, K. E. Sanwald, A. S. Crampton, C. J. Ridge, F. Jäckel, J. Feldmann, M. Tschurl, U. Heiz, *J. Am. Chem. Soc.,* 2013, **135**, 13262-13265; (b) T. Wu, Q. Zhang, Y. Hou, L. Wang, C. Mao, S.T. Zheng, X. Bu, P. Feng, *J. Am. Chem. Soc.,* 2013, **135**, 10250-10253.